Smart Electrical Grid Interface Using Floating H-Bridges to Improve the Performance of Induction Motors

A. R. N. M. Reaz Ul Haque, Siyu Leng, and John Salmon, *Member, IEEE*

***Abstract*—Three-phase floating H-bridges can be inserted between the utility grid and an induction motor to inject a voltage in series with the grid voltage. The magnitude and phase of this voltage is used to control the motor voltage under steady-state operation so as to lower the motor power losses over its entire load range. This is made possible because the three-phase H-bridge can be used to both increase and decrease the motor voltage relative to the grid voltage as required. This feature affects the performance of the overall system, more specifically, the motor power conversion efficiency is improved, lowering its operating temperature and, hence, improving reliability and lifetime expectancy. A variety of motor voltage control options exist, the controller presented is suitable for applications using loads such as fans and pumps, where variable frequency is not required. Readily available machine nameplate data are used to identify the motor output power associated with its maximum efficiency operating point when operated under rated voltage. This data are then used as the basis to control the motor voltage according to the square root of the measured motor input power. The controller and the performance of the three-phase H-bridge are described. The benefits of the variable voltage control are assessed by comparing the motor performance with the machine operated at its rated voltage. The chosen controller also results in the H-bridge dc voltages being relatively low and constant over a wide load range, hence lowering the power losses and electrical stress in the power electronics. Both experimental results and theoretical predictions are used to illustrate the performance of both the three-phase H-bridge and the motor.**

***Index Terms*—Floating capacitor, H-bridge converters, induction motor, reactive power generation, series compensation.**

I. Introduction

THE three-phase induction motor is the workhorse of modern industry. Worldwide about 50 million motors are installed every year [1] and approximately 50% of electrical energy produced is used in electric drives. Typically, 60–80% of the electricity in the industrial sector and about 20–35% of the electricity in the commercial sector is consumed by motors [2].

Manuscript received July 12, 2016; revised October 20, 2016; accepted November 16, 2016. Date of publication December 1, 2016; date of current version May 9, 2017. Recommended for publication by Associate Editor J. Zhang.

A. R. N. M. R. Haque and J. Salmon are with the Department of Electrical and Computer Engineering,University of Alberta, Edmonton, AB T6G 2V6, Canada (e-mail: arnmreaz@ualberta.ca; john.salmon@ualberta.ca).

S. Leng is with the Department of Electrical Engineering,Petroleum Institute, Abu Dhabi, UAE (e-mail: sleng@pi.ac.ae).

Color versions of one or more of the figures in this paper are available online at http://ieeexplore.ieee.org.

Digital Object Identifier 10.1109/TPEL.2016.2633978

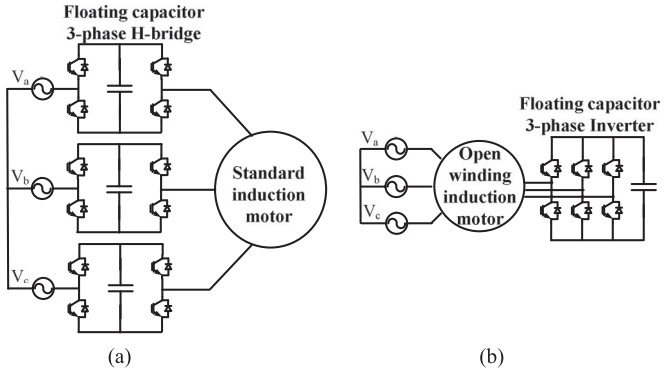

Fig. 1. Power electronic converters for series voltage compensation of a smart grid connected induction motor: (a) three-phase H-bridge and (b) three-phase inverter.

Around 67% of this energy, and representing 85% of all motor energy losses, is associated with induction motors with a rating below 75 kW [3], [4]. Hence, the energy efficiency and reliability of grid connected induction motors are a major interest from both economic and environmental perspectives.

The electronic operating systems used with many induction motors are a significant element in future industrial smart grids, used as a means to achieve energy savings, reduce production costs, and provide grid voltage support: one popular system is a variable frequency drive (VFD) [5], [6]. Considering that many applications operate induction motors continuously at full speed, e.g., fans and pumps, for these situations, lower cost power electronics can be considered that supply the motor at fixed frequency. The power electronic systems can be used to control the motor voltage under a variety of situations [7], [8]: limit the motor starting current; provide immunity to grid voltage sags and swells; generate VARs into the grid for VAR compensation and voltage support; provide a buffer between the motor mechanical system and the grid to limit system oscillations; and lastly, to control the motor voltage to lower its energy losses. The latter feature is the subject of this paper, using a transformer less three–phase floating H-bridge system [see Fig. 1(a)] with Fig. 1(b) being an alternative option.

Many loss minimization control schemes for induction motors have been reported [9], [10]. These techniques can be divided into three main categories: 1) model-based methods; 2) simple state control; and 3) search control.

Calculation intensive model-based methods provide smooth and fast adaptation of the motor flux as long as the motor parameters are known, e.g., rotor speed or slip, core loss, main inductance saturation [11]. The less complex state control assumes certain quantities of the motor can be easily defined, such as displacement power factor or slip to operate motor at maximum efficiency. Alternatively, rotor slip frequency control requires a speed feedback. The constant power factor approach has a relatively fast response ($<$1 s) and is a good choice for industrial drives [12]. A real-time search method can be used to find the motor voltage that minimizes the motor input power for a constant load output power [13], [14]. Theoretically, this method offers an optimal solution; however, this method is not popular as it has a slow response to load changes ($>$7 s) [15], difficulties tuning the algorithm, and requiring precise load information.

The operation and performance of a three-phase floating H-bridge is presented [see Fig. 1(a)] that controls the motor voltage using a series voltage injection relative to the fixed frequency grid voltage. The proposed system using 12 switches can be considered more energy efficient and cost effective when compared to other systems such as a standard VFD and a regenerative drive, or back-to-back (BTB) converter. The benefits of the three-phase H-bridge over the standard VFD and the BTB converter are discussed in [16]. The standard VFD uses a six-switch output inverter with a diode rectifier input stage, and so may be considered more economic? However, the overall system power losses and costs are higher due to: 1) large input current harmonics flowing through the drive input diode rectifier and ac reactor; 2) large bulky 3/5% reactors are often included at the input and output: note that replacing iron with silicon is often considered advantageous; 3) the standard VFD requires a higher dc-link voltage in continuous operation than the proposed system (e.g., 290 versus 200 V in a 208-V three-phase system), hence increases the inverter losses. The higher system losses in the standard VFD increase the cost of the cooling systems [16]. A BTB converter uses 12 switches, similar to the proposed system, and has the advantage of motor variable frequency control [17]–[20]. However, the three-phase H-bridge is not being proposed for variable frequency applications but for applications where continuous operation from a fixed utility frequency is the main operating condition for the machine. BTB converters operate from a higher dc-link voltage than the proposed system (e.g., 290 versus 200 V in a 208-V three-phase system). The higher dc voltage produces higher steady-state losses in the power electronics, increasing the cooling requirements and cost. The three-level line input and output voltages, using a larger dc-link voltage, of the BTB converter requires larger input and output filters: the proposed system can produce five-level pulse width modulation (PWM) line voltages with smaller voltage steps and a PWM frequency double that of the BTB converter. Hence, the proposed system can be considered more cost competitive because of the lower cooling and ac filter requirements.

Comparisons between floating H-bridge topologies and alternative systems are described in [16] and [21]. A "magnetic energy recover switch" switches at the ac supply frequency and is mainly used for VAR compensation [22]–[24]. The system has many disadvantages including large current harmonics and undesirable system oscillations [24]. A hybrid cascaded converter using floating H-bridges can be used with an NPC to control the system VARs [25], [26]. Leng *et al.* [21] describe the use of the three-phase floating H-bridge as a series compensator to decouple the motor voltage from grid voltage sags and swells. The system naturally produces a leading power factor at the grid and generates VARs. Leng *et al.* [16] describe how the three-phase floating H-bridge can be used to soft-start an induction motor using motor voltage control.

In contrast to [16] and [21], the main contribution of the work presented is to show how a grid connected three-phase floating H-bridge can be used to improve the continuous steady-state operation of an induction motor operating at the grid frequency (see Fig. 1).

The three-phase H-bridge version [see Fig. 1(a)] is the preferred implementation for many industrial applications as the three-phase inverter [see Fig. 1(b)] requires an open winding machine with the inverter operating at twice the dc-link voltage in comparison. However, the motor loss minimization control presented is designed for implementation using either of the floating bridges illustrated in Fig. 1. The motor variable voltage control presented is intended to operate the motor at its maximum power conversion efficiency, using machine nameplate data as input parameters and the measured motor input power to determine the demand voltage for the controller. This approach is intended for applications where frequency control is not required, such as fans, pumps, compressors, and some applications using medium voltage motors [21]. The motor efficiency can be improved over the entire motor load range, from no-load to full-load, as the floating power electronics can increase or decrease the motor voltage relative to the grid voltage. The results of extensive experimental performance testing of the motor and system as a whole compare very favourably with theoretical predictions.

II. Motor Voltage Control

Two voltage control modes were chosen to highlight the benefits of variable voltage control using the three-phase H-bridge over operating the motor at its rated voltage: 1) "*rated voltage control*," V_{rated} and 2) "*variable voltage control*", V_{var}. The former control keeps the motor voltage constant at rated irrespective of grid voltage droops, sags or swells or motor load condition. The latter control requires the motor voltage to be greater than or less than the grid voltage and is chosen to minimize the motor losses, hence maximize the motor power conversion efficiency. The rated grid voltage is assumed to be the same as the motor rated voltage and the motor load is assumed to vary over a wide range, typically from 10% to 100% of rated.

Variable voltage control is based upon the electrical per-phase equivalent circuit of the induction motor under steady-state conditions and neglecting temperature and saturation effects. Note that the motor is operated with a constant supply frequency under low slip conditions. The maximum motor efficiency condition is estimated from nameplate data and is associated with the motor rated voltage V_{mo}, motor input impedance Z_{ph}, and input power P_{mo}. The motor voltage is then changed as the

square root of the measured electrical input power $P_{\rm in}$ relative to $P_{\rm mo}$. As the motor power changes, the motor input impedance $Z_{\rm ph}$ stays constant together with the input power factor, slip and rotor speed

$$V_m = V_{\rm mo}\sqrt{\frac{P_{\rm in}}{P_{\rm mo}}}. \tag{1}$$

For illustrative purpose, this section uses the following equivalent circuit parameters for an induction motor: 230 V, 60 Hz, 5 HP (3.7 kW), 1760 r/min, four poles, $\eta = 91\%$, 0.83 PF, 12.5 A, $R_s = 0.62\,\Omega$, $R_r = 0.26\,\Omega$, $X_s = 0.50\,\Omega$, $X_r = 0.752\,\Omega$, $X_m = 20\,\Omega$, and $R_m = 1058\,\Omega$.

An induction motor with these parameters has a maximum power conversion efficiency of 91% occurring at roughly 65% of the motor rated load. This setting can then be used to define a nominal input power $P_{\rm mo}$ and motor voltage $V_{\rm mo}$.

The three-phase H-bridge differs from previous methods reported [14], [27] as the motor voltage can be made to be greater than the grid voltage to improve the motor efficiency at high loads, and less than the grid voltage to improve the motor efficiency under light loads: details of the three-phase H-bridge control are given in Sections III and V. Fig. 2(a) compares rated voltage control versus variable voltage control using (1). Variable voltage control results in the motor power factor being constant at approximately 0.71, compared with rated voltage control, where the power factor varies from 0.83 at full load, down to 0.1 under light load. Noting that the three-phase H-bridge provides a series voltage injection V_b at 90° to the current, see Section III-A, then the per-unit injected voltage $V_{b,\rm pu}$ is shown in Fig. 2(b) as a function of the motor voltage $V_{m,\rm pu}$ using curves at motor power factor angles ϕ_m in 10° steps: $V_{b,\rm pu}$ for $V_{\rm rated}$ and $V_{\rm var}$ control are also highlighted in the figure. Significantly, variable voltage control, $V_{\rm var}$, largely results in a lower injected voltage, $V_{b,\rm pu}$. [see Fig. 2(b)]. This can be used advantageously to lower the power losses and electrical stresses in the power electronics by lowering the dc voltages in the three-phase H-bridges.

Variable voltage control theoretically results in the motor efficiency staying at the motor maximum over the entire load range [see Fig. 2(c)], note that motor resistance variation with temperature are ignored in this observation. Rated voltage control results in much lower power conversion efficiencies under both high and light loads. These trends in the efficiency curves are reflected in the motor current and machine loss curves [see Fig. 2(d) and (e)]. Unlike rated voltage control, variable voltage control maintains a balance between the current flowing through the motor magnetizing inductance and its rotor circuit. This balance lowers the motor input current under both light load and high load conditions, hence lowering the motor losses.

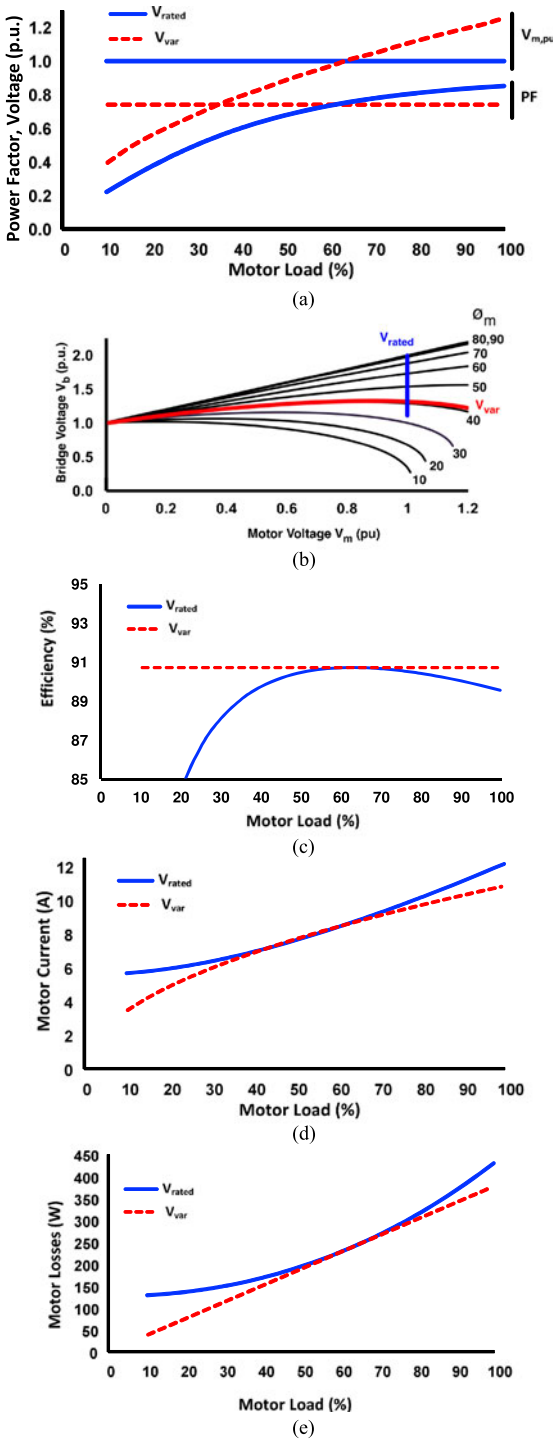

Fig. 2. Motor operation under rated and variable voltage control: (a) motor voltage and power factor, (b) bridge voltage as a function of the motor power factor angle, (c) motor efficiency, (d) motor current, and (e) motor losses.

III. Three-Phase H-Bridge Control

For the three-phase H-bridge to deliver the desired motor voltage, a motor voltage larger, equal to, or less than the grid voltage is required. For this voltage to be sustainable in steady state, the injected voltage V_b has to be approximately at 90° to the current: losses in the power electronics change this angle slightly. Control of V_b, hence V_m, is achieved by changing the voltage injection angle α relative to the grid voltage [16], [21]. The system fundamental voltage vectors required to achieve the two modes of motor voltage control are presented. Theoretical analysis of the vector diagrams is presented to predict both angle α and magnitude of the injected voltage V_b. Performance curves for the three-phase H-bridge are presented for both motor

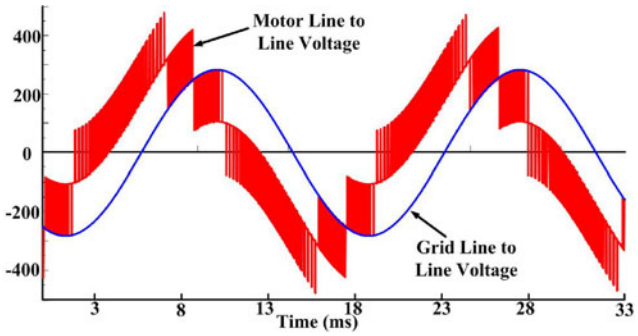

Fig. 3. Motor line voltage component due to the H-bridges.

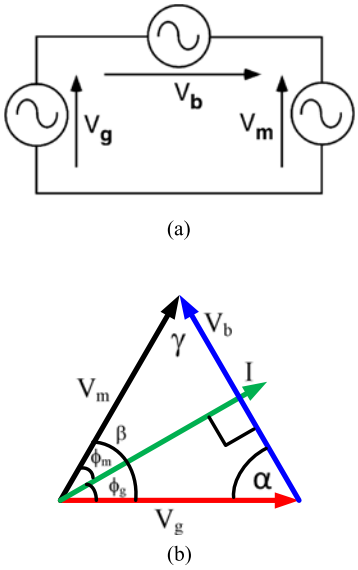

Fig. 4. Simplified system fundamental voltage single phase representation: (a) equivalent circuit and (b) vector diagram with angles labeled.

control modes. Lastly, the motor parameters stated in Section II are assumed here.

A. Series Voltage Injection

The three-phase floating H-bridges inject three-level PWM voltages in each motor phase with a fundamental component, V_b. Two H-bridge voltage waveforms add with the grid line voltage to form the line voltage delivered to the motor (see Fig. 3): two H-bridge voltages result in a five-level PWM voltage in the motor line voltage with a PWM frequency up to four times the bridge switching frequency. The fundamental component of the motor line voltage, V_{Lm}, determines the fundamental phase voltage delivered to the motor and is denoted V_m, with the per-phase component of the grid voltage denoted V_g, where the line grid voltage is denoted as V_{Lg} and is rated as 230 V ($V_{\mathrm{Lg}} = 230\,\mathrm{V}$; $V_g = 133\,\mathrm{V}$). The fundamental voltages can be represented in a per-phase equivalent circuit [see Fig. 4(a)] and a per phase voltage vector diagram [see Fig. 4(b)]. Various angles are identified in Fig. 4(b) for analysis purposes. One important feature to note from the vector diagram is that in steady state the bridge voltage V_b is at 90° to the motor current I_m, representing no net power flow to the H-bridge capacitors.

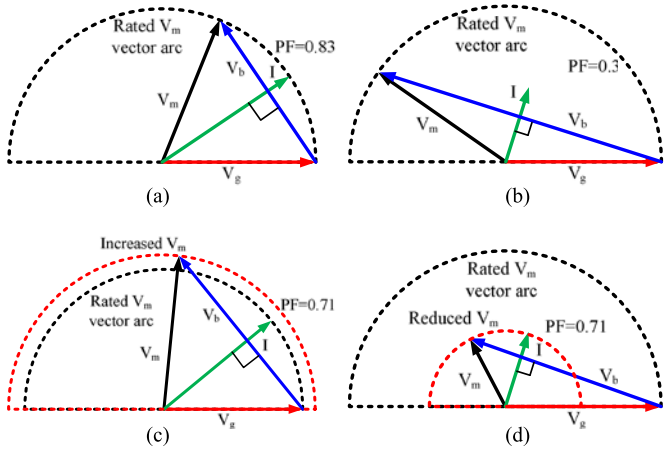

Fig. 5. Phasor voltage vectors: (a) $V_m = \mathrm{rated}$, high load, (b) $V_m = \mathrm{rated}$, light load, (c) $V_m > \mathrm{rated}$, high load, (d) $V_m < \mathrm{rated}$, light load.

Given the motor parameters stated in Section II, the voltage injection angle α [see Fig. 4(b)] can be controlled to deliver the desired motor voltage V_m to the motor. When adopting rated voltage control, V_m follows a semicircle [see Fig. 5(a) and (b)] in the voltage vector diagram, and α is changed to keep V_m fixed as the motor power factor changes: 0.83 at full load [see Fig. 5(a)] down to 0.3 under light load [see Fig. 5(b)]. Alternatively for variable voltage control, the motor power factor is fairly constant, 0.71 in Fig. 5(c) and (d). Under high load, the motor voltage has to be boosted above rated [see Fig. 5(c)] and reduced under light load [see Fig. 5(d)], as given by (1). The vector diagrams in Fig. 5 demonstrate that the three-phase H-bridge can deliver the desired motor voltage by changing α as long as the bridge capacitor voltage is allowed to change: the amplitude modulation depth m_{a} of the H-bridges is fixed at its maximum to minimize dc capacitor operating voltage.

B. Voltage Vector Analysis

As the motor load changes, the motor characteristics determines the relationship between the motor voltage V_m, fundamental power factor $\cos\phi_m$, and power factor angle ϕ_m [see Fig. 2(a) and (b)]: the grid voltage V_g is assumed constant and the same as the motor rated voltage V_{rated}. During the steady-state operation, the system power factor angle as seen at the grid ϕ_g, H-bridge fundamental voltage V_b, and the resultant dc voltage V_{dc} can be predicted knowing V_g, V_m, and ϕ_m.

For simplification, assume

$$V_{m,\mathrm{p.u.}} = \frac{V_m}{V_g}. \tag{2}$$

Using Fig. 4(b), ϕ_g and α are obtained from

$$\cos\phi_g = V_{m,p.u.}\cos\phi_m \tag{3}$$

$$\sin\alpha = V_{m,\,\mathrm{pu}}\cos\phi_m \tag{4a}$$

$$\cos\alpha = \frac{V_g^2 + V_b^2 - V_m^2}{2V_gV_b}. \tag{4b}$$

Knowing ϕ_g, ϕ_m the remaining angles in the vector diagram Fig. 4(b) are obtained using:

$$\beta = \phi_m + \phi_g \tag{5a}$$

$$\gamma = 90 - \phi_m . \tag{5a}$$

Using the motor parameters stated in Section II, α is illustrated in Fig. 6(a) as a function of the motor load in %. For completeness, γ and β are shown in Fig. 6(b). Noting that the motor decides the relationship between V_m and ϕ_m as the motor load changes, ϕ_m and ϕ_g are shown in Fig. 6(c). Interestingly, both control modes have α changing relatively close together increasing from under 10° at light load to close to 50°–60 ° at high load. The controller (see Section V) uses α to deliver the desired motor voltage and Fig. 5 gives an insight as to how this is possible. For rated voltage control, the motor power factor is low under light load and high under high load [see PF in Fig. 2(a) and ϕ_m in Fig. 6(c)]. Hence, α is low under light load and high at high load [see (4a)]. Conversely for variable voltage control, the motor power factor is constant but the motor voltage is low under light load and high at high load, see PF in Fig. 2(a) and ϕ_m in Fig. 6(c). Hence, considering Fig. 5, α changes from a small value under light load to a high value under high load.

The linear relationship between cos ϕ_g with $V_{m,\mathrm{pu}}$ and cos ϕ_m [see (3)], accounts for the decreasing magnitude of ϕ_g as the load increases in Fig. 6(c) for both control cases. Note that ϕ_g is a leading angle relative to V_g, while ϕ_m is a lagging angle relative to the V_m. For rated voltage control $V_{m,\mathrm{pu}}$ is constant, but ϕ_m decreases with increasing load, hence ϕ_g decreases also. For variable voltage control, ϕ_m is constant, but ϕ_g decreases with increasing load as $V_{m,\mathrm{pu}}$ increases with increasing load [see (3) and (1)].

With the various angles defined and assuming $V_g = V_{\mathrm{rated}}$, the bridge injected voltage V_b can be predicted using Fig. 4(b), and can be expressed in two ways:

$$V_b = V_g \frac{\cos(\alpha - \phi_m)}{\cos(\phi_m)} = \sqrt{V_g^2 - (V_m \cos\phi_m)^2} + V_m \sin\,\phi_m . \tag{6}$$

The capacitor dc voltage is minimized by keeping the bridge PWM amplitude modulation depth m_a at maximum, resulting in the bridge capacitor voltage fluctuating with V_b, and given by

$$V_{\mathrm{cap}} = \frac{\sqrt{2} V_b}{m_a}. \tag{7}$$

V_{cap} is plotted in Fig. 6(d) for both control cases assuming $V_{\mathrm{Lg}} = 230\,\mathrm{V}$ for the 5 HP/ 3.7 kW machine described in Section II. An obvious benefit of the variable voltage control, operating with a constant relatively low power factor of 0.71, is that the capacitor voltage is fairly constant as the load changes and peaks at just over 200 V as compared with 340 V for the rated voltage control. This has many benefits in lowering the power electronics losses and electrical stresses, hence lowering temperature fluctuations.

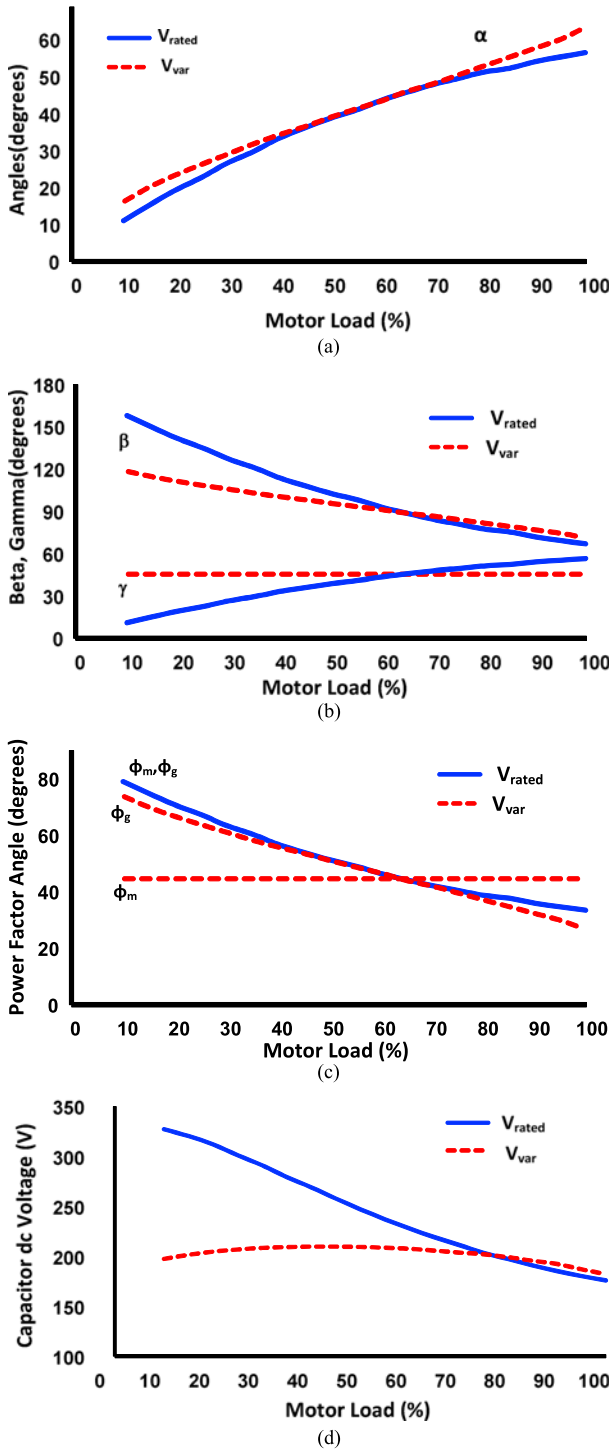

Fig. 6. Rated and variable voltage control: (a) control angle α, (b) angles γ and β, (c) grid and motor displacement angles ϕ_g and ϕ_m , and (d) capacitor dc voltage.

For rated voltage control: (3), (4) gives

$$\cos\phi_g = \cos\phi_m \Rightarrow \mathrm{PF}_g = \mathrm{PF}_m \tag{8}$$

$$\sin\alpha = \cos\phi_m . \tag{9}$$

$$\text{Hence, } V_{b,\,\mathrm{pu}} = 2\,\sin\,\phi_m . \tag{10}$$

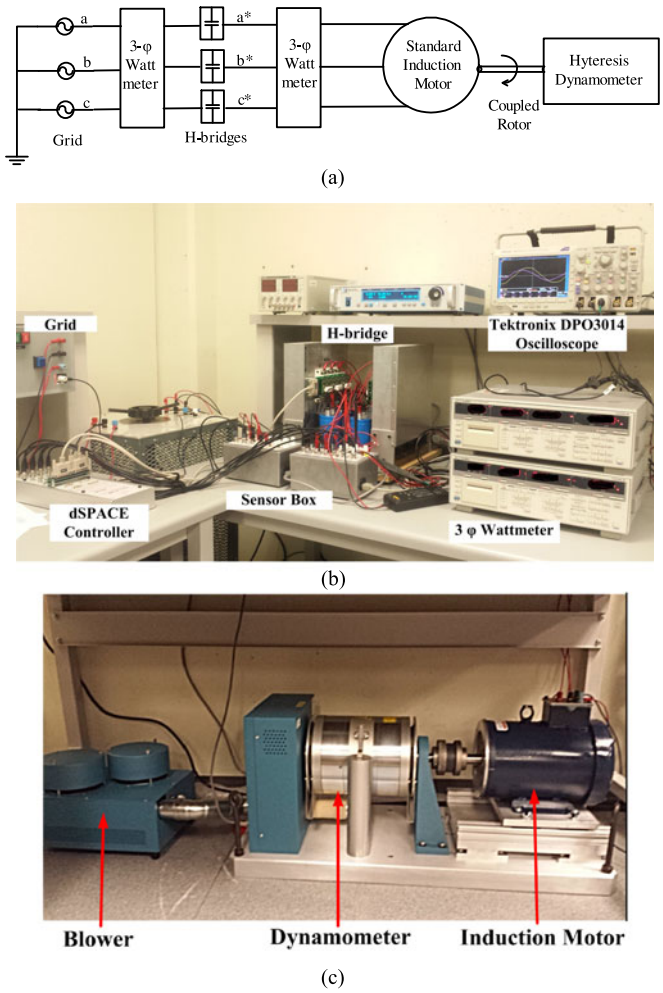

Fig. 7. Experimental setup: (a) block diagram, (b) three-phase H-bridge system with a dSPACE controller, and (c) induction motor with dynamometer.

For variable voltage control assuming: $\cos\phi_m = 0.71$:

$$\cos\,\phi_g = \frac{V_{m,\,\mathrm{pu}}}{\sqrt{2}},\ \sin\,\alpha = \frac{V_{m,\,\mathrm{pu}}}{\sqrt{2}}. \tag{11}$$

$$\text{Hence},\, V_b = \sqrt{1 - \left(\frac{V_{m,\,\mathrm{pu}}}{\sqrt{2}}\right)^2} + \frac{V_{m,\,\mathrm{pu}}}{\sqrt{2}}. \tag{12}$$

These expressions are useful in determining the theoretical system and motor performance when the motor characteristics are known: e.g., system VARs, power factor, and bridge capacitor dc voltage stresses.

IV. Experimental Setup

A 230-V 5-HP (3.7 kW) motor-dynamometer system was used as the test platform, schematically shown in Fig. 7(a). Three single-phase H-bridges are inserted between the grid and the induction motor. A dynamometer is mechanically coupled with the induction motor: the experimental test facility is shown in Fig. 7(b) and (c).

The converters used in the experiment are custom made using Semikron (SKiM306GD12E4) IGBT modules. The H-bridges

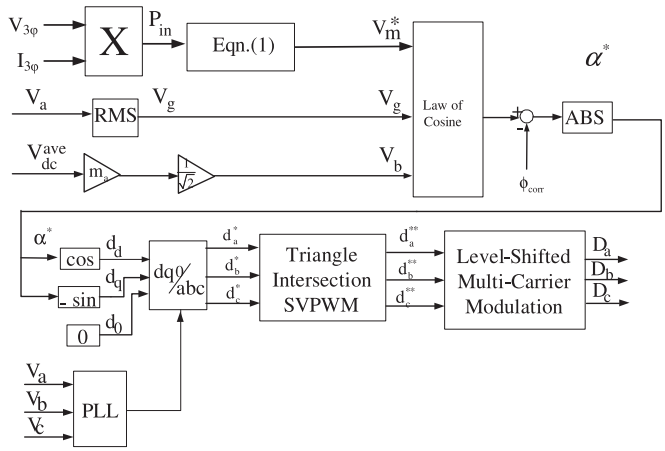

Fig. 8. Control block diagram for variable motor voltage control.

were made up of two separate inverter legs each using two 4-mF 500-V rated capacitors connected in parallel. Note that the capacitors were part of a general purpose lab system and smaller values can be used with a 5 HP (3.7 kW) motor.

The MAGTROL hysteresis dynamometer was used as a load, with a frictionless torque loading, independent of the shaft speed. Loading of the dynamometer is controlled by a MAGTROL DSP 6000 dynamometer controller so that a constant load torque can be provided. The dSPACE controller had the following input/output settings: 1) the dSPACE algorithm in the CLP1104 platform was limited to 200-μs computing times, resulting in a 5-kHz signal sampling rate and using a low-pass filter. This was deemed sufficient to obtain the rms of 60-Hz currents and voltages as verified using separate meters and 2) the two dSPACE CLP1104 PWM blocks are difficult to synchronize. Specific PWM frequencies have to be used and the chosen 7.5 kHz was one such frequency. The resulting 15-kHz PWM frequency was also exactly three times the signal sampling period.

A 230-V, 1760 r/min, four pole, 90.7%, 0.85 PF, 60 Hz, 5 HP (3.7 kW), 12.25 A, induction machine was used for experimental testing and its equivalent circuit parameters, neglecting temperature effects, were determined as being: $R_s = 0.65\,\Omega$, $R_r = 0.26\,\Omega$, $X_s = 0.74\,\Omega$, $X_r = 0.9\,\Omega$, $X_m = 23.08\,\Omega$, and $R_m = 750\,\Omega$. Nameplate data stated that out of three settings (50%, 75%, 100% load), the motor is the most efficient at 75% load, 0.75 PF, 230 V, and 90.5% efficiency. The experimental controller used this 75% load data as the nominal setting for the motor maximum efficiency in the variable voltage control; see V_{mo} and P_{mo} in (1).

V. Motor Voltage Control

Motor voltage control is achieved by changing the control angle α^* (see Fig. 8). In general, the higher the value of α^*, the higher is the motor voltage and vice versa. More specifically, using a PLL and knowing V_g together with V_{cap}, then the controller can set α to supply the motor at its demand voltage, V_m^*. For rated voltage control, V_m^* corresponds to the motor rated

voltage ($V_{\rm rated} = V_g$), for variable voltage control, V_m^* is given by (1) to keep the motor operating at maximum efficiency.

The input power $P_{\rm in}$ for (1) is measured at the grid side, though strictly this measurement also includes the power losses in the power electronics. The grid voltage is used by the controller PLL to provide the base reference frame for phase information. Both the current and voltage feedback signals measured at the grid side are reliable low-noise signals.

The rms value of the grid voltage V_g can be measured easily using two line voltages. The three-phase H-bridge capacitor voltages naturally have a low-frequency ripple (120 Hz). These ripple voltages tend to cancel each other when the average of the three bridge dc voltages is used to derive the signal voltage to represent $V_{\rm cap}$ $(= V_{\rm dc}^{\rm ave})$. The H-bridge dc capacitor voltages are allowed to vary and steady state is reached when the bridge voltage is at 90° to the motor current. Switching and conduction losses change this angle slightly depending upon the relative load power level. Note that Fig. 6(d) shows that the proposed variable voltage control maintains a relatively constant capacitor voltage. This is caused by the power factor of the machine also being held fairly constant as a result of the controller used.

The higher the modulation index, the lower the dc capacitor voltage. Therefore, the amplitude modulation depth of the three phase bridges is set to its maximum to minimize the bridge dc voltages, and so the injected fundamental voltage V_b is estimated using (7): note that theoretically $m_{a,\max} = 1.15$ but 1.12 was used experimentally.

A PLL is used to track the grid voltage angle (θ), which is used to perform the inverse Park's transformation converting the *dq0* frame modulation signals d_d, d_q, d_0 into the *abc* frame signals d_a^*, d_b^*, d_c^*. The demand motor voltage V_m^* is translated into the actual motor voltage V_m using the control signal α^* calculated using (4b) [see Fig. 8]. Triangle intersection implementation of space vector pulse width modulation is used to obtain the PWM reference signals d_a^{**}, d_b^{**}, d_c^{**}, hence zero sequence triplen harmonic signal components are present. Finally, comparison with level-shifted multicarrier signals yields the gating signals D_a, D_b, D_c for the H-bridges [28], hence producing five-level PWM line voltage waveforms [16], [21].

VI. Experimental Results

The system performance is compared over a wide load range between using rated voltage control ($V_{\rm Lm} = 230\,{\rm V}$; $V_m = 133{\rm V}$) and variable voltage control ($V_m = V_{\rm var}$). The motor with the basic motor parameters defined in Section IV was used for testing. However, the theoretical motor performance curves were improved from those shown in Section II as the motor equivalent circuit resistances were adjusted with the motor operating temperature for each load setting. Better agreement between experimental and theoretical predictions was achieved as a result. Section VI-E describes the relationship between the motor losses and its temperature rise. In this paper, direct method in the IEC 60034-2-1 [29] and Method A in IEEE Standard 112 [30] is used to determine motor efficiency.

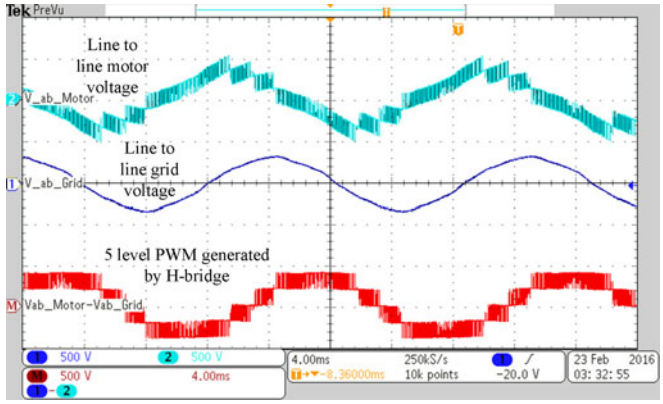

Fig. 9. Experimental three-phase voltages: motor and grid line, 2 H-bridge voltages.

A. Five-Level Motor Line Voltage

The three-phase H-bridges generate three-level PWM voltage outputs resulting in five-level PWM line voltages at frequencies up to four times the switching frequency (see Fig 9). These PWM waveforms have smaller step sizes than experienced in a standard VFD and produce lower noise and cable interaction problems.

B. General Motor Performance

Good agreement was obtained between experimental and theoretical motor performance predictions for all the parameters presented in Fig. 10. The results confirm that the motor voltage controller illustrated in Fig. 8, and using α control as defined in (4b), is a good method for directly controlling the motor voltage [see Fig. 10(a)].

Variable voltage control improves the motor efficiency at both high and light load levels, reducing the motor current and lowering the motor losses. For example, 7% reduction of the motor current is obtained under full load and 11% reduction under light load [see Fig. 10(b)]. The two controllers produce similar results in the mid power range as expected.

Variable voltage control has a steadily decreasing efficiency as the motor power is increased [see Fig. 10(c)] compared with the flat characteristics in Fig. 2(c). This is caused by the temperature dependence of the motor resistance with the motor load. The motor efficiency for rated voltage control peaks at around the 60% load level. This implies that if motor data are available, then the variable voltage control would use the motor parameters at this setting rather than the 75% load from the motor nameplate data. The variable voltage experimental currents, power losses, and efficiency show good agreement between experimental and theoretical predicted results. The same parameters for rated voltage control are in close agreement with slightly higher differences.

Under light load, variable voltage control has a motor efficiency of 92% as compared to 79% under rated voltage control; the difference in efficiency at full load is approximately 1%. Higher power conversion efficiencies are associated with lower motor losses and a lower temperature rise: an approximate 15%

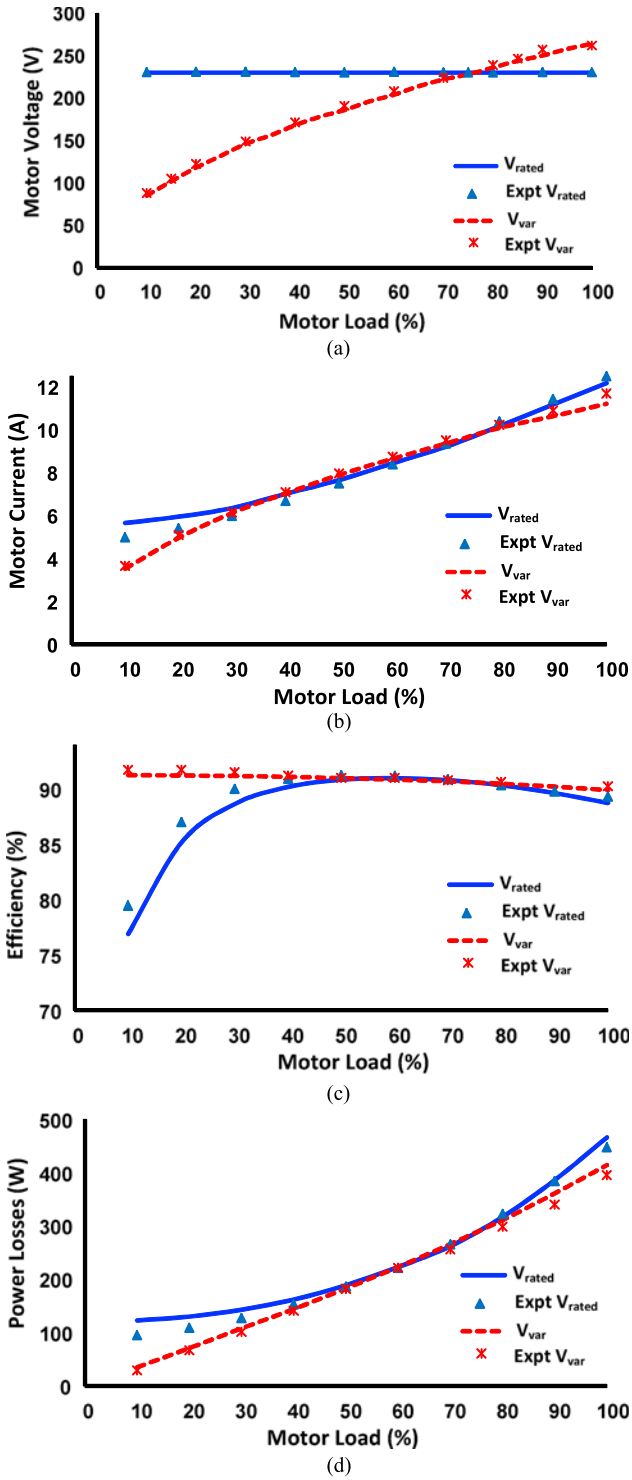

Fig. 10. Motor performance as a function of the motor output load in %. (a) Motor voltage, (b) motor current, (c) efficiency, and (d) motor power losses.

loss reduction is possible at rated load. Variable voltage control increases the motor rating by approximately 7% as a result of the lower losses [see Fig. 10(d)]. This increases the motor lifetime expectancy: note that the motor winding insulation life can be doubled for every 10°C reduction in average operating temperatures [31]. Accurate motor voltage control using the three-phase

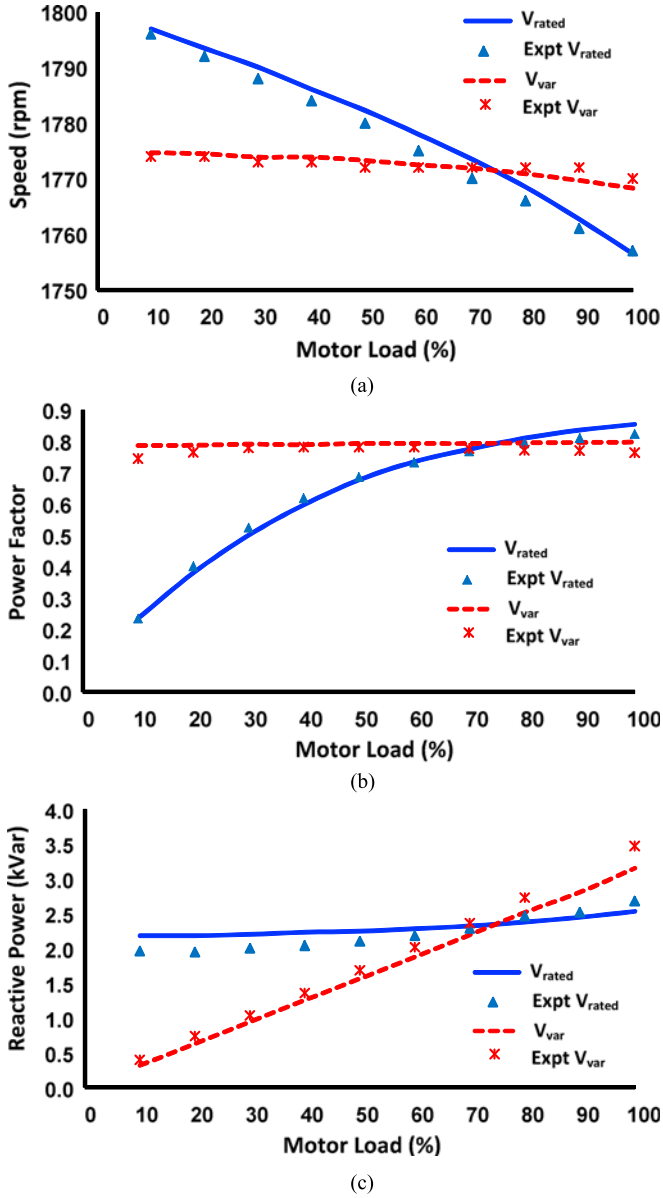

Fig. 11. Motor reactive power and speed: (a) rotor speed, (b) power factor, and (c) reactive power.

H-bridge means that the motor is also immune to grid voltage sags and swells. Grid voltage fluctuations often require a derating of the motor power [32] and using a motor with a larger frame size [33].

C. Motor Reactive VARs and Rotor Speed

Variable voltage control is associated with the machine having a relatively constant input impedance, constant speed, and constant power factor. The experimental results presented in Fig. 11 confirm these conclusions with a good agreement between experimental and theoretical predictions. For instance, the motor power factor is fairly constant and close to 0.75–0.8, with experimental results giving slightly lower values [see Fig. 11(c)]. The motor reactive VARs demand decrease linearly with decreasing

load since the motor is also operating at constant power factor [see Fig. 11(b)].

Rated voltage control has a droop in speed with increasing load commonly associated with induction motors operated at constant voltage [see Fig. 11(a)]: the motor droop in power factor as the load is decreased is also a classic characteristic associated with induction motors [see Fig. 11(b)]. The motor operating at almost constant reactive VARs under rated voltage control is caused by the magnetizing inductance drawing a constant current [see Fig. 11(c)].

D. Grid Power Factor and VARs Generation

The three-phase H-bridge voltage injection V_b phase shifts the motor voltage V_m so that it leads the grid voltage V_g. This results in the motor current leading V_g, hence generating VARs into the grid instead of consuming [see Fig. 12(a)]. The grid power factor decreases with a decreasing motor load for both controllers [see Fig. 12(b)]. However, the grid power factor is leading rather than the lagging power factor at the motor terminals. This can be expected for rated voltage control since $|\phi_g| = |\phi_m|$ when $V_m = V_g$ and ϕ_g leads with ϕ_m lagging [see Fig. 4(b)]. For rated voltage control, the motor VARs demand is relatively constant, hence the grid VARs generation is also relatively constant [see Figs. 12(c) and 4(b)]. For variable voltage control, first, the system power factor decreases linearly with the motor load as expected. Second, since the machine impedance is assumed constant and the motor voltage changes according to the square-root of the motor power, then the grid current hence grid apparent power changes according to the square root of the motor power. These two trends for the grid power and apparent power result in the curved relation for the grid VARs generation relative to the motor load [see Fig. 12(c)].

E. Temperature Dependence

The motor temperature rise is widely assumed to be proportional to its power losses. Experimental tests results prove this to be the case for the motor used in this study. The stator temperature rise is the most significant as the stator winding insulation lifetime deteriorates with temperature. The stator temperature rise was obtained by operating the motor from a 230-V supply for a few hours at each power setting, stopping and measuring the stator winding resistance within 30 s of cutting the power to the machine. A linear relationship between the motor losses and temperature rise was obtained, with the motor rising to 60 °C at the motor rated conditions of 5 HP (3.7 kW) and 230 V, respectively [see Fig. 13(a)]: the data for the machine quoted a 65 °C rise under rated conditions. The power losses obtained for both the rated and variable voltage control were then related to the stator temperature rise using the results from Fig. 13(a) [see Fig. 13(b)]. The stator temperatures coincide in the mid motor load region, as expected from the maximum efficiency condition used to set up the controller. Under rated power conditions ($\text{Torque} = 20\ \text{N}\cdot\text{m}$), the variable voltage control produced a temperature rise of 7.5 °C less than rated voltage control, corresponding to a 75% increase in stator winding insulation lifetime expectancy according to [31]. Under light load

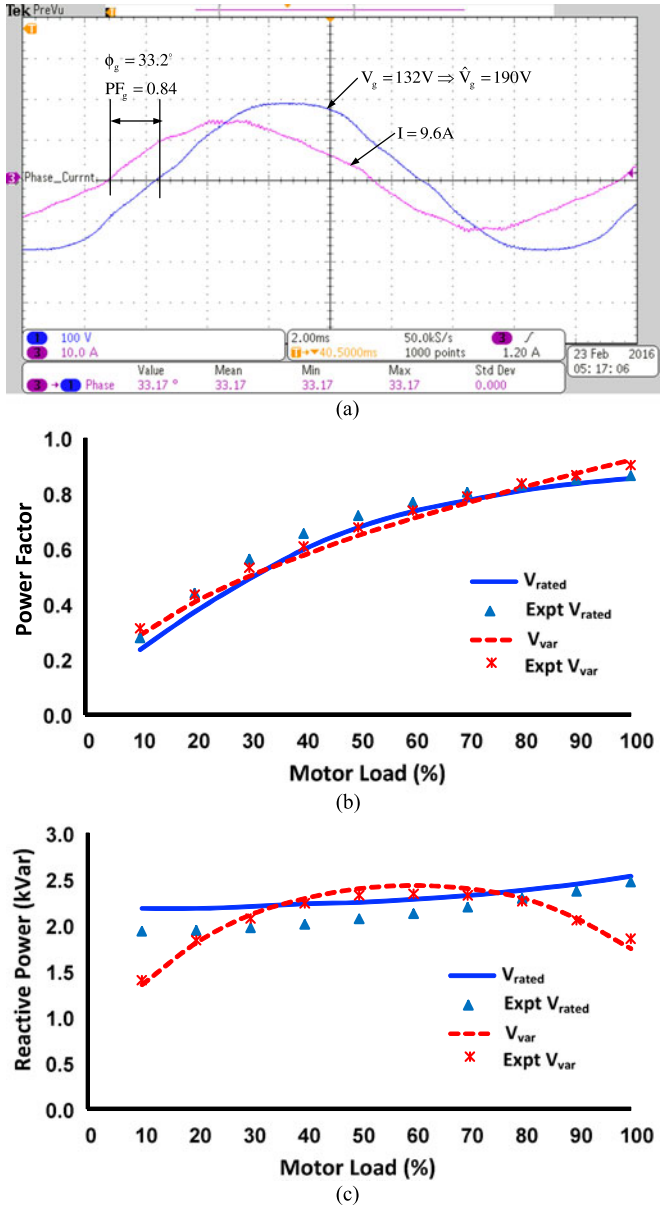

Fig. 12. Reactive VAR generation and grid Power Factor: (a) leading grid current, (b) grid power factor (PF_g), and (c) grid VAR generation.

($\text{Torque} = 2\ \text{N}\cdot\text{m}$), the variable voltage control produced a temperature rise 10 °C less than rated voltage operation, representing a 100% increase in winding insulation lifetime if the machine were operated under this load continuously; however, this result if for a very light load is less significant, than the full-load result. Considering the same temperature rise obtained under rated power conditions for variable voltage control, rated voltage control produces approximately 7% less power: this represents a 7% power derating.

F. DC Voltage Reduction

The average H-bridge dc capacitor voltage can be predicted using (6) and (7) and is illustrated in Fig. 2(b) via observing V_b. Relatively close agreements between predicted and

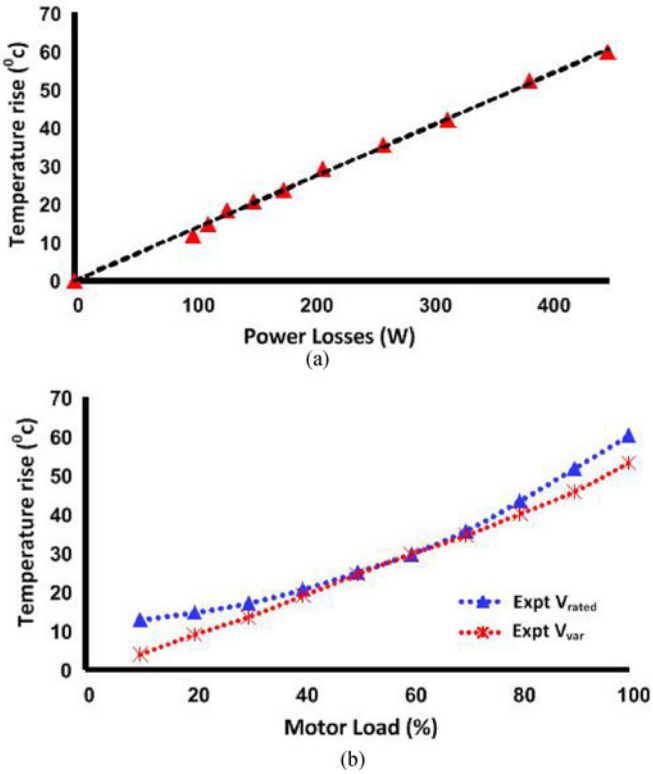

Fig. 13. Motor stator temperature rise dependence on losses: (a) stator temperature as a function of motor losses ($V_{\mathrm{Lm}} = 230$ V) and (b) temperature rise comparison between rated and variable motor voltage.

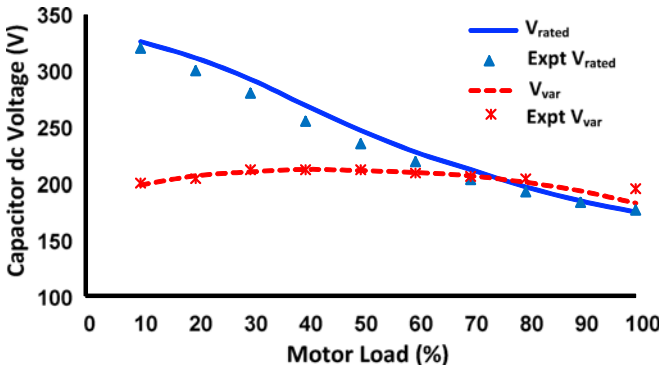

Fig. 14. Comparison of dc capacitor voltage.

experimentally measured values were obtained (see Fig. 14). Variable voltage control produces a relatively constant capacitor dc voltage over the full motor load range, whereas rated voltage control results in a wide variation, increasing with decreasing load. The latter characteristics are caused by the motor power factor decreasing with the motor load [see Figs. 2(a), (b) and 6(d)]. The relatively constant bridge dc voltage for variable voltage control is related to the motor operating with a relatively constant load power factor as the motor load changes. The relatively low bridge dc voltage, close to 200 V, is advantageous as it produces lower stress on the power electronics and decreases its losses.

VII. Conclusion

The performance of a three-phase H-bridge system using floating dc capacitors is presented for a smart utility grid interface for induction motors. The proposed system is intended to be used in applications such as fans, pumps, compressors, and medium voltage motors, where variable frequency control is not required [16], [21]. A variable motor voltage control is described that is based upon maximizing the motor operating efficiency by controlling the motor voltage to be proportional to the square root of the measured motor input power. The controller was implemented using input parameters based upon readily available machine data, such as the motor performance at 75% output power, corresponding to the maximum known motor efficiency condition without having to use more detailed motor modelling. The proposed variable voltage control produced high motor power conversion efficiency over a wide load range, together with reduced power losses and lower rms currents. The machine speed was shown to be relatively constant over a wide load range. The system naturally produces a leading grid power factor, hence generates VARs in to the grid. Comparing variable voltage control with rated voltage control, the motor temperature was reduced by 7.5 °C at the motor rated output power, and 10 °C lower under light load. Lastly, the variable voltage controller results in the H-bridge dc voltages to be relatively constant as the load changes at much lower levels than obtained when operating under-rated voltage. This reduces the electrical stresses on the power electronics and improves their reliability and lifetime expectancy. For applications where frequency control is not required, the proposed three-phase H-bridge system is a viable reliable cost-effective alternative.

References

[1] K. Berringer, J. Marvin, and P. Perruchoud, "Semiconductor power losses in AC inverters," in *Proc. 30th IAS Annu. Meeting Ind. Appl. Conf. Rec.*, Oct. 8–12, 1995, vol. 1, pp. 882–888.

[2] A. T. de Almeida Fernando and F. Ferreira, "Efficiency testing of electric induction motors," vol. 2, ISR, Dep. Eng. Electronica University of Coimbra, Polo 1997, p. 3030.

[3] M. Kostic and B. Kostic, "Motor voltage high harmonics influence to the efficient energy usage," in *Proc. Invited Paper 15th WSEAS Int. Conf. Syst.*, Corfu Island, Greece, Jul. 2011, pp. 276–281.

[4] P. S. Hamer, D. M. Lowe, and S. Wallace, "Energy-efficient induction motors-performance characteristics and life-cycle cost comparison for centrifugal loads," in *Proc. Inst. Elect. Electron. Eng. Incorporated Ind. Appl. Soc. 43rd Annu. Petroleum Chemical Ind. Conf. Rec. Conf. Papers*, Sep. 23–25, 1996, pp. 209–217.

[5] H. N. Hickok, "Adjustable speed-A tool for saving energylosses in pumps, fans, blowers, and compressors," *IEEE Trans. Ind. Appl.*, vol. IA-21, no. 1, pp. 124–136, Jan. 1985.

[6] S. V. Giannoutsos and S. N. Manias, "A data-driven process controller for energy-efficient variable-speed pump operation in the central cooling water system of marine vessels," *IEEE Trans. Ind. Electron.*, vol. 62, no. 1, pp. 587–598, Jan. 2015.

[7] F. Blaabjerg, J. K. Pedersen, S. Rise, H.-H. Hansen, and A. M. Trzynadlowski, "Can soft-starters help save energy?" *IEEE Ind. Appl. Mag.*, vol. 3, no. 5, pp. 56–66, Sep./Oct. 1997.

[8] T. M. Rowan and T. A. Lipo, "A quantitative analysis of induction motor performance improvement by SCR voltage control," *IEEE Trans. Ind. Appl.*, vol. IA-19, no. 4, pp. 545–553, Jul. 1983.

[9] F. Abrahamsen, "Energy optimal control of induction motor drives," Ph.D. dissertation, Dept. Energy Technol., Aalborg Univ., Aalborg, Denmark, 2000.

[10] A. M. Bazzi and P. T. Krein, "Review of methods for real-time loss minimization in induction machines," *IEEE Trans. Ind. Appl.*, vol. 46, no. 6, pp. 2319–2328, Nov./Dec. 2010.

[11] S. Lim and K. Nam, "Loss-minimising control scheme for induction motors," *IEEE Proc. Elect. Power Appl.*, vol. 151, no. 4, pp. 385–397, Jul. 2004.
[12] F. J. Nola, "Power factor control system for AC induction motor," U.S. Patent 4 052 648, Oct. 4, 1977.
[13] A. Kusko and D. Galler, "Control means for minimization of losses in AC and DC motor drives," *IEEE Trans. Ind. Appl.*, vol. IA-19, no. 4, pp. 561–570, Jul./Aug. 1983.
[14] D. S. Kirschen, D. W. Novotny, and T. A. Lipo, "Optimal efficiency control of an induction motor drive," *IEEE Trans. Energy Convers*, vol. EC-2, no. 1, pp. 70–76, Mar. 1987.
[15] F. Abrahamsen, F. Blaabjerg, J. K. Pedersen, P. Z. Grabowski, and P. Thogersen, "On the energy optimized control of standard and high-efficiency induction motors in CT and HVAC applications," *IEEE Trans. Ind. Appl.*, vol. 34, no. 4, pp. 822–831, Jul./Aug. 1998.
[16] S. Leng, R. Ul Haque, N. Perera, A. Knight, and J. Salmon, "Soft start and voltage control of induction motors using floating capacitor H-bridge converters," *IEEE Trans. Ind. Appl.*, vol. 52, no. 4, pp. 3115–3123, Jul./Aug. 2016.
[17] R. Cuzner, D. Drews, and G. Venkataramanan, "Power density and efficiency comparisons of system-compatible drive topologies," *IEEE Trans. Ind. Appl.*, vol. 51, no. 1, pp. 459–469, Jan./Feb. 2015.
[18] E. Wemekinck, A. Kawamura, and R. Hoft, "A high frequency ac/dc converter with unity power factor and minimum harmonic distortion," in *Proc. 7th IEEE Power Electron. Spec. Conf.*, 1987, pp. 264–270.
[19] A. Reznik, M. G. Simoes, A. Al-Durra, and S. M. Muyeen, "*LCL* filter design and performance analysis for grid-interconnected systems," *IEEE Trans. Ind. Appl.*, vol. 50, no. 2, pp. 1225–1232, Mar./Apr. 2014.
[20] M. Liserre, F. Blaabjerg, and S. Hansen, "Design and control of an LCL-filter-based three-phase active rectifier," *IEEE Trans. Ind. Appl.*, vol. 41, no. 5, pp. 1281–1291, Sep./Oct. 2005.
[21] S. Leng, R. Haque, N. Perera, A. Knight, and J. Salmon, "Smart grid connection of an Induction motor using a 3-phase floating H bridge system as a series compensator," *IEEE Trans. Power Electron.*, vol. 31, no. 10, pp. 7053–7064, Oct. 2016.
[22] T. Isobe *et al.*, "Improved performance of induction motor using magnetic energy recovery switch," in *Proc. Power Convers. Conf.*, Nagoya, Japan, 2007, pp. 919–924.
[23] F. Danang Wijaya, S. A. Kusumawan, and H. Prabowo, "Reducing induction motor starting current using magnetic energy recovery switch (MERS)," in *Proc. 6th Int. Conf. Inf. Technol. Elect. Eng.*, Oct. 7–8, 2014, pp. 1–6.
[24] J. A. Wiik, F. D. Wijaya, and R. Shimada, "Characteristics of the magnetic energy recovery switch (MERS) as a series FACTS controller," *IEEE Trans. Power Del.*, vol. 24, no. 2, pp. 828–836, Apr. 2009.
[25] M. Veenstra and A. Rufer, "Control of a hybrid asymmetric multilevel inverter for competitive medium-voltage industrial drives," *IEEE Trans. Ind. Appl.*, vol. 41, no. 2, pp. 655–664, Mar./Apr. 2005.
[26] C. Silva, L. A. Cordova, P. Lezana, and L. Empringham, "Implementation and control of a hybrid multilevel converter with floating DC links for current waveform improvement," *IEEE Trans. Ind. Electron.*, vol. 58, no. 6, pp. 2304–2312, Jun. 2011.
[27] D. S. Kirschen, D. W. Novotny, and W. Suwanwisoot, "Minimizing induction motor losses by excitation control in variable frequency drives," *IEEE Trans. Ind. Appl.*, vol. IA-20, no. 5, pp. 1244–1250, Sep. 1984.
[28] B. Wu, *High-Power Converters and AC Drives*. New York, NY, USA: Wiley-IEEE Press, Mar., 2006, ch. 7.
[29] *Rotating Electric Machines Part 2-1: Standard Methods for Determining Losses and Efficiency from Tests*, IEC 60034-2-1, 2007.
[30] *IEEE Standard Test Procedure for Polyphase Induction Motors and Generators*, in IEEE Std 112-2004 (Revision of IEEE Std. 112-1996), pp. 0_1–79, 2004.
[31] A. H. Bonnett, "Reliability comparison between standard and energy efficient motors," *IEEE Trans. Ind. Appl.*, vol. 33, no. 1, pp. 135–142, Jan./Feb. 1997.
[32] T. A. Jankowski *et al.*, "Development and validation of a thermal model for electric induction motors," *IEEE Trans. Ind. Electron.*, vol. 57, no. 12, pp. 4043–4054, Dec. 2010.
[33] H. Li and R. S. Curiac, "Designing more efficient large industrial induction motors by utilizing the advantages of adjustable-speed drives," *IEEE Trans. Ind. Appl.*, vol. 46, no. 5, pp. 1805–1809, Sep./Oct. 2010.

A. R. N. M. Reaz Ul Haque received the B.Sc. degree in electrical and electronics engineering (EEE) from the Bangladesh University of Engineering and Technology, Dhaka, Bangladesh, and the M.Sc. degree in power system from the University of New Brunswick, Fredericton, NB, Canada. He is currently working toward the Ph.D. degree under the supervision of Dr. John Salmon, University of Alberta.

He was a Lecturer at North South University, Bangladesh. His research interests include motor drives, voltage balancing for hybrid vehicle, and multilevel converter.

Siyu Leng (M'14) received the B.Sc. degree in automation from Tongji University, Shanghai, China, in 2006. He was granted a full scholarship from the Florida State University to study in the USA. He received the Ph.D. degree in 2012.

During the Ph.D. degree, he joined the Center for Advanced Power Systems (CAPS) as a Graduate Research Assistant under the supervision of Prof. David A. Cartes. His research at CAPS was focused on power quality, especially active power filters. After receiving the Ph.D. degree, he went back to China to work as a Research Engineer at State Grid Electric Power Research Institute. Since May 2013, he has been a Postdoctoral Fellow at the University of Alberta, Edmonton, AB, Canada, under the supervision of Prof. John Salmon. His research at the University of Alberta was focused on power electronics, especially induction motor drives. He joined Petroleum Institute as a Research/Teaching Associate in October, 2014. His research interests include: renewable energy, power electronics, motor drive, power quality, and power system analysis.

John Salmon (S'86–M'86) received the B.Sc.Eng. degree from Imperial College London, London, U.K., in 1982, the M.Eng. degree from McGill University, Montreal, QC, Canada, in 1984, and the Ph.D. degree from Imperial College London in 1987.

In 1987, he became an Assistant Professor in the Department of Electrical Engineering, University of Alberta, Edmonton, AB, Canada, where he has been a Full Professor since 1996. He has conducted industrially funded power-electronics research projects covering a wide range of applications, such as electronic ballasts for fluorescent lamps and metal-halide high-intensity discharge lamps, utility interface of micro turbine generators using high-speed permanent magnet generators, medium-voltage industrial drive systems, and soft starters for medium-voltage induction motors. His current research interests include industrial drive systems and their utility interface multipulse utility rectifiers, multilevel voltage-source converters, high-speed ac drive systems, coupled inductor inverters, floating bridge power electronics for motor control applications, battery voltage balancing networks, and multifunctional pulsewidth-modulated converters.

Dr. Salmon received three Prize Paper Awards from the IEEE Industry Applications Society: third prize from the Industrial Drives Committee in 1994, first prize from the Industrial Drives Committee in 2008 and first prize from the Industrial Power Converter Committee in 2010.